European Journal of Pharmaceutics and Biopharmaceutics 144 (2019) 180–192

Contents lists available at ScienceDirect

European Journal of Pharmaceutics and Biopharmaceutics

journal homepage: www.elsevier.com/locate/ejpb

Research paper

Unidirectional drug release from 3D printed mucoadhesive buccal films using FDM technology: *In vitro* and *ex vivo* evaluation

Georgios K. Eleftheriadis[a], Christos Ritzoulis[b], Nikolaos Bouropoulos[c,d], Dimitrios Tzetzis[e], Dimitrios A. Andreadis[f], Johan Boetker[g], Jukka Rantanen[g], Dimitrios G. Fatouros[a,*]

[a] Department of Pharmacy, Aristotle University of Thessaloniki, 54124 Thessaloniki, Greece
[b] Department of Food Science and Technology, International Hellenic University, Sindos Campus, 57400 Thessaloniki, Greece
[c] Department of Materials Science, University of Patras, 26504 Rio, Patras, Greece
[d] Foundation for Research and Technology Hellas, Institute of Chemical Engineering and High Temperature Chemical Processes, 26504 Patras, Greece
[e] International Hellenic University, School of Science and Technology, 14km Thessaloniki - N. Moudania, Thermi GR57001, Greece
[f] Department of Oral Medicine/Pathology, School of Dentistry, Aristotle University of Thessaloniki, Thessaloniki, Greece
[g] Department of Pharmacy, University of Copenhagen, Universitetsparken 2, DK-2100 Copenhagen, Denmark

ARTICLE INFO

Keywords:
3D printing
FDM
Buccal
Mucoadhesion
Chitosan
Diclofenac
Unidirectional
Backing layer

ABSTRACT

Oromucosal delivery of active pharmaceutical ingredients provides an attractive alternative route of administration, due to avoidance of the first pass effect and improved patient compliance. In the current work, fused deposition modelling (FDM) 3D printing was investigated as an additive manufacturing approach for poly(vinyl alcohol)-based mucoadhesive films, enabling unidirectional drug release. For this purpose, chitosan was incorporated as a permeation and mucoadhesion enhancer whereas ethylcellulose and commercial wafer sheets were evaluated as backing layers. The formulated films were initially assessed for structural integrity and dose uniformity. Solid-state characterization of the films, including thermal methods (DSC, TGA), diffraction (XRPD) and Raman spectroscopy, was implemented to characterize the physicochemical properties of the produced polymeric filaments and buccal films. The mechanical properties of the products were investigated by instrumented indentation and tensile tests. Evaluation of buccal films was assessed *in vitro*, to study the effect of backing-layer type on hydration capacity of the films, diffusion of the drug throughout the restricting layer and release profiles in simulated saliva. The *ex vivo* performance of the manufactured products, associated with the presence of chitosan, was investigated by textural analysis for mucoadhesion properties, whereas permeation studies and histological studies were performed across porcine buccal epithelium. The results demonstrated that FDM printing is a timesaving and versatile approach in the context of manufacturing multi-layered mucoadhesive buccal films, providing unidirectional release properties.

1. Introduction

In the last decade, additive manufacturing (e.g. 2D and 3D printing) has been utilized in the development of orally delivered dosage forms, as well as oromucosal drug delivery systems [1,2]. Fused deposition modelling (FDM) is the most often applied 3D printing technique. Development of a thermoplastic filament *via* hot melt extrusion (HME) is required, and the printing process is based on sequential deposition of molten-polymer layers, according to predetermined digital patterns. Additionally, FDM printing is the method of choice for manufacturing of pharmaceutical dosage forms, due to cost effectiveness, printing speed and a constantly growing number of pharmaceutical-grade polymers available as feeding materials [3,4]. Moreover, versatility of the digitally-designed patterns facilitated 3D printing of complex structures, providing advanced performance of the dosage forms. Thus, tablets or capsular devices of various shapes and internal structures have been developed, to facilitate controlled release profiles [5–10], targeted drug delivery [11–13] and compartmental inclusion of active ingredients or drug loaded carriers [13–16]. Orodispersible and fast-dissolving oral films were additionally prepared by FDM printing for the oral delivery of active compounds, exhibiting fast-dissolving properties [17,18]. Furthermore, a 3D printed wearable device was investigated in the first-in-human study for topical delivery of active compounds in the oral cavity [19].

Alternative sites of administration could benefit by exploitation of the unique advantages of FDM printing. For example, the buccal

* Corresponding author.
E-mail address: dfatouro@pharm.auth.gr (D.G. Fatouros).

https://doi.org/10.1016/j.ejpb.2019.09.018
Received 9 April 2019; Received in revised form 20 September 2019; Accepted 20 September 2019
Available online 21 September 2019
0939-6411/

mucosa provides a competent route of administration, due to avoidance of the hepatic first pass effect of drugs with low bioavailability, and improved patient compliance due to the geometric characteristics of films (compared to tablets). In the context of manufacturing of buccal films, there are critical features that must be considered, i.e. mucoadhesion, drug permeation through the oral epithelium, and regulation of drug release. The permeability barrier of the buccal mucosa is located in the upper epithelial region [20]. Considering the high concentration of polar lipids in the intercellular space, drug permeation is accomplished either across the cells (transcellular route) or by passive diffusion through the intercellular space (paracellular route) in the case of lipophilic or hydrophilic molecules, respectively [20,21]. Thus, lipophilicity (logP), distribution coefficient (logD) and molecular weight of the active compound are crucial features that should be considered in the context of development of buccal formulations [22–24]. To enhance the permeability of active compounds through the buccal epithelium, penetration enhancers are incorporated in the composition of the dosage form. Their action is based on increased partitioning of the drug in the epithelium, extraction of intercellular lipids and disruption of the tight protein junctions [25]. Natural or synthetic mucoadhesive polymers are often used to increase the residence time of formulations on the administration site and optimize localized drug delivery, whereas application of a backing layer facilitates unidirectional release of the drug and avoidance of drug swallowing [26,27]. The perspective of developing oral films *via* printing technologies has been widely discussed in the literature [1,28].

Solvent casting and hot melt extrusion are conventional manufacturing methods for buccal films [29]. The solvent casting method consists of several steps; though, the most time-consuming step is the drying process of the casted solution, as drying periods of 6–48 h are commonly reported [29–32]. Specific structural properties of buccal films, capable of providing functional characteristics (i.e. backing layers, drug loaded reservoirs and mucoadhesive layers) are usually achieved through multi-step processes [33–35]. Moreover, films prepared by solvent casting and hot melt extrusion techniques need to be manually cut, to prepare appropriate formulation size, dose or shape [36–38].

In the current work, FDM printing was employed as a timesaving and versatile alternative approach, for the development of mucoadhesive buccal films. Poly(vinyl alcohol) has been widely used in pharmaceutical and biomedical applications, and has been reported to provide excellent film forming properties [35], highly thermoplastic properties and excellent printability [4,10,39]. Thus, poly(vinyl alcohol)-based films were fabricated for the buccal delivery of a model hydrophilic drug, i.e. diclofenac sodium. Xylitol was incorporated in the polymer blend as plasticizer. Polymeric filaments and buccal films were formulated in absence or presence of chitosan, to investigate the effect of the natural polymer on mucoadhesion and drug permeation. The capabilities of FDM printing were further utilized to develop multi-layered films. Formulations incorporating a backing layer were manufactured, in the context of modifying the drug release properties. Ethyl cellulose, plasticized by triethyl citrate, and commercial wafer edible sheet were evaluated as backing layers to facilitate unidirectional release of the drug. The compositional- and structural-driven hypothesis was investigated by physicochemical and mechanical studies, as well as by *in vitro* and *ex vivo* evaluations.

2. Materials and methods

2.1. Materials

Poly(vinyl alcohol) (PVA, Mowiol 4-88, Mw ~ 31000), chitosan (CS, low molecular weight) and triethyl citrate (TEC) were purchased from Sigma-Aldrich, Germany. Diclofenac sodium (DNa) and xylitol (Xyl) were purchased from Fagron Hellas, Greece. Ethyl cellulose (EC, Ethocel Std 45) was kindly supplied by Rontis Hellas S.A., Greece. Wafer paper edible sheets (WAF) were purchased from Kopyform GmbH, Germany. All other materials and reagents were of analytical grade.

2.2. Preparation of filaments

Polymeric filaments were produced by a Filabot Original single-screw extruder (Filabot Inc., VT, USA). The % content of raw materials was selected in a way that plasticization of the polymers occurred efficiently and feeding in the printhead did not induce extensive deformation or breakage of the filaments [13,40,41]. Thus, the composition of feeding powder-mixtures for drug-loaded filaments in absence (0C-filament) or presence (1C-filament) of chitosan was PVA:Xyl:CS:DNa 78:14:0:8 or 77:14:1:8 (% w/w) respectively, whereas the EC- filament providing the backing-layer comprised of EC:TEC 90:10 (% w/w). The extrusion temperature was 169 °C with a 1.40 mm nozzle diameter for PVA, and 165 °C with 1.60 mm nozzle diameter for EC-filaments. The nozzle diameters were selected to minimize deviations from the acceptable diameter's range of the produced filaments, due to the die swelling effect [42] and in combination with morphological observations.

2.3. Development of 3D printed buccal films

The formulations of the study were divided in two main groups, regarding the content of CS, with the abbreviations of 0C (absence) and 1C (1% presence of CS). Considering the presence and the type of backing layer, these groups were further divided in three subgroups, i.e. X-formulations (no backing layer), EC-formulations (backing layer of ethylcellulose) and WAF-formulations (backing layer of commercial edible wafer sheet). To investigate the effect of these factors on the overall performance of the formulations, six different buccal films namely; 0C-X, 1C-X, 0C-EC, 1C-EC, 0C-WAF and 1C-WAF were developed by 3D printing.

The digital templates of buccal films were designed in Autocad 2019 (Autodesk Inc., USA) and exported as stereolithography files (.stl). Drug loaded films were 3D printed in a Makerbot Replicator 2X FDM printer (Makerbot Inc., USA). The templates of films without a backing layer were designed as 20x20 mm rectangles with a thickness of 0.2 mm. The patterns of drug loaded specimens comprised of a four-layered crosswise sequence, with a 50 μm layer height each. Since the layer height exceeded the manufacturer's recommended z-axis resolution, re-calibration of the building platform at proper positions was mandatory. Furthermore, a 45° rotation value (z-axis) was set, to avoid potential defects on the connection points of infill-printed lines with the bounded outline-shell (n = 1), associated with the diagonal infill printing direction (on x-y orientation) as illustrated in Fig. S1.

In the case of the EC backing layer, an additional 20 × 20 × 0.1 mm square item was printed on the top surface of the drug loaded films and the layer height was set at 100 μm. Utilization of WAF as backing layer was implemented by applying the commercial edible sheets on the building platform. Manual calibration of the platform height was performed prior to printing the drug loaded films onto the edible surface. Post-printing, the WAF sheet was manually cut according to the edges of the 3D printed patterns by using a surgical blade, to facilitate isolation of the drug loaded films with WAF backing.

The extrusion temperatures were set to 200 °C and 190 °C for PVA and EC filaments respectively, whereas the platform was heated to 80 °C. All printing speeds were reduced to 10 mm/s with 100% infill. The filament diameter was set in the software in accordance with the extrusion nozzle diameter incorporated in hot melt extrusion, the morphological assessment of the filaments, and the manual caliper measurements.

2.4. Quantification of the active compound

A high performance liquid chromatography (HPLC) system, consisted of an LC-10 AD VP pump, a SIL-20A HT autosampler and a UV − vis SPD-10A VP detector, was utilized in the study for the quantification of DNa [43]. In brief: stationary phase, Discovery RP Amide C16 column (15 cm, 4.6 mm, 5 μm); mobile phase, (A) acetonitrile, (B) KH_2PO_4 0.025 M, pH 3 adjusted with phosphoric acid (50:50 v/v, A:B). Vacuum degas (20 min) and sonication (10 min) of the mobile phase was performed prior to all measurements. The flow rate was set at 1.0 mL/min, whereas an injection volume of 20 μL and 50 μL was used for *in vitro* and *ex vivo* studies respectively. A 276 nm wavelength, combined with 15 min sample runtime, resulted in DNa detection at 10.5 min. Standard DNa samples were tested over the range of 0.1–100 μg/mL ($R^2 \geq 0.999$).

2.5. Preliminary evaluation

Films of each formulation type (n = 10) were evaluated for weight uniformity. Additionally, each film was dissolved in 20 mL distilled water under stirring. An aliquot of the solution was withdrawn in 1 h, centrifuged at 4000 rcf for 10 min and analyzed by HPLC to determine the API content for each formulation (n = 5).

2.6. Physicochemical characterization

Scanning electron microscopy (SEM) was utilized in the study, to evaluate the morphological characteristics of the developed polymeric filaments and buccal films, using a Zeiss SUPRA 35VP SEM microscope (Zeiss, Oberkochen, Germany).

Thermal analysis of raw materials, filaments and formulations was conducted by thermogravimetric analysis (TGA) using a TA Q500 Thermogravimetric Analyzer (TA Instruments, New Castle, DE, USA). Approximately 10 mg of the investigated materials and samples were placed in platinum pans. Thermograms were recorded in the range 35–500 °C, with a heating rate of 10 °C/min.

Complemental thermal analysis was performed by Differential Scanning Calorimetry (DSC) in a DSC 204 F1 Phoenix instrument (Netzsch, Selb, Germany). Samples of 5–10 mg were placed in aluminum pans, and the thermal properties were monitored with a 10 °C/min heating rate. Thermograms were obtained in a temperature range that complied with the extrapolated thermal degradation onset temperatures obtained by TGA studies.

The X-ray powder diffraction (XRPD) patterns of raw materials and samples were recorded with a D8-Advance instrument (Bruker, Germany), using Cu $K_{\alpha 1}$ radiation at 40 kV and 40 mA. The diffraction range was 5-50° 2θ, the step size was 0.02° and the scanning speed was set at 0.35 s/step. Raman spectroscopy measurements were conducted in a Raman RXN1 spectrometer (Kaiser Optical Systems, Ann Arbor, MI, USA). The Raman shift was recorded in the range 500–1900 cm^{-1}, with a 785 nm laser wavelength. Spectra of raw materials and formulations were accumulated 5 times with a 4 s exposure.

2.7. Mechanical tests

2.7.1. Instrumented indentation tests

Formulations 0C-X and 1C-X of buccal films, as well as plain wafer paper and ethyl cellulose printed layer were assessed through indentation tests, to compare their elastic modulus and hardness. In instrumented indentation tests the load is measured as a function of penetration depth. In the current work the indentations were conducted using a dynamic ultra-micro-hardness tester (DUH-211, Shimadzu Co., Kyoto, Japan) fitted with a triangular pyramid indenter tip (Berkovich indenter). The indentations made on the surface of the films under study appeared as an equilateral triangle. The indentation hardness was automatically converted to Vickers hardness by the software of the apparatus. Ten measurements were conducted on each specimen which were purposely scattered on the surface. After contact with the surface, the indenter was driven into the surface up to a peak load of 10 mN. To minimize the effect of viscoelastic deformation of the specimen on property measurements, notably creep, the peak load was held for 3 s and the indenter was withdrawn to zero load.

2.7.2. Tensile tests

Tensile tests were performed at room temperature on a Testometric (UK) universal testing machine equipped with a 1 KN load cell at a constant crosshead speed of 0.5 mm/min. The modulus was calculated within the linear part of the stress–strain curves. All presented data correspond to the average of at least four measurements.

2.7.3. Folding endurance

The folding endurance of the developed 3D printed formulations was determined by repeatedly folding the films at the same plane until rupture occurred or folding to 300 times without breaking [44].

2.8. In vitro evaluation

2.8.1. Evaluation of backing layers

The ability of backing layers to provide unidirectional release properties on the developed formulations was investigated (n = 3) in a Side-Bi-Side diffusion cell (PermeGear, Inc., USA), with 5 mL internal donor/acceptor chamber volume and an orifice diameter of 5 mm. Each one of the proposed backing layers (3D printed EC layer and wafer edible sheet) was mounted between the diffusion compartments, and the set-up temperature was equilibrated at 37 °C. DNa was solubilized (1 mg/mL) in simulated saliva fluid (SSF) (sodium chloride 0.8%, potassium phosphate (monobasic) 0.019%, sodium phosphate (dibasic) 0.238% (w/v), pH 6.8) [45]. The drug-loaded solution (5 mL) was placed in the donor chamber, whereas the acceptor chamber was filled with drug-free SSF (both preheated at 37 °C). Samples of 200 μL were withdrawn from the acceptor compartment at predetermined time intervals for 180 min. The API was quantified by HPLC to calculate the diffusion steady-state mass flux (J_{ss}) from the slope of the cumulative mass-time plotted curve (linear fraction) and assess the performance of backing layers. The lag time of diffusion was determined from the intersection of the linear fitted curve with the time-axis.

2.8.2. Water-uptake

A gravimetric approach was followed to evaluate the degree of hydration of the formulated films, using a VTI-SA Vapor Sorption Analyzer. Samples of the formulated materials (ca. 10 mg) were placed in the sample holder and a drying stage at 60 °C and 0% relative humidity (RH) was initiated for 3 h. Subsequently, the %weight alterations of samples (equilibrium criteria, 0.001% in weight change in 5 min) were recorded at 25 °C and at predetermined RH intervals in the range 10–95%.

2.8.3. Release studies

The DNa release from the developed formulations was investigated in SSF (n = 3) as following: double-wall glass vessels were filled with 50 mL SSF and allowed to equilibrate at 37 °C. The SSF volume was selected in a way that the buccal films were completely immersed in the release medium and the effect of the presence or type of backing layer could be monitored. Reported solubility data of DNa in purified water and SSF confirmed the maintenance of sink conditions throughout the timespan of the study [43,46]. Each formulation was fitted in custom-made metal-wire frames, immersed in the vessel, and positioned at 2/3 of the medium's total height. Magnetic stirring at 50 rpm was applied. Samples of 2 mL were withdrawn from the release medium at predetermined time intervals for 120 min, and the vessels were immediately replenished with equal volumes of fresh SSF, preheated at 37 °C. The samples were centrifuged at 4000 rcf for 10 min and

Table 1
Weight and dose uniformity data of the developed formulations in absence or presence of chitosan (0C or 1C) and absence or presence of a backing layer (X: absence, EC: ethylcellulose, WAF: wafer).

Formulation	0C-X	1C-X	0C-EC	1C-EC	0C-WAF	1C-WAF
Film weight [mg]	112.8 ± 2.1	113.4 ± 1.9	151.9 ± 2.2	152.4 ± 2.5	181.9 ± 8.9	176 ± 9.6
Drug content [mg]	9.10 ± 0.21	9.04 ± 0.26	8.92 ± 0.24	9.01 ± 0.26	9.05 ± 0.30	8.98 ± 0.25

analyzed by HPLC. Modelling of the release profiles was implemented in SigmaPlot v.12.5 (Systat Software, Inc., Chicago, IL, USA) by exploitation of a curve fitting library (release.jfl). The release data were fitted in three kinetic models (first order, Korsmeyer-Peppas and Hixson-Crowell) to determine the equation parameters and the drug release mechanism.

2.9. Ex vivo evaluation

2.9.1. Mucoadhesion studies

The mucoadhesive properties of the fabricated formulations were determined utilizing a TA-XT texture analyzer (TA instruments, New Castle, DE) (n = 4). In detail, the 3D printed films and polyethylene terephthalate (PET) films were mounted on the device probe and platform respectively, by using double-adhesive tape. Freshly excised (< 2h) porcine buccal mucosa was attached with cyanoacrylate glue on PET films. After spreading 0.1 mL SSF onto the mucosa, the probe was lowered at 0.5 mm/s speed to maintain contact of the formulation with the subjacent mucosa for 120 s (applied force 0.5 g). Afterwards the probe was withdrawn at 1 mm/s speed and the force-distance curves were recorded. The maximum detachment force (F_{max}) was detected as the maximum force applied to completely detach the formulated film from the buccal mucosa, whereas the work of adhesion (W_{ad}) was calculated from the area under the curve in the force-distance plot.

2.9.2. Permeation studies

Permeation of the API across freshly excised (< 2h) porcine buccal mucosa was investigated at 37 °C in Franz diffusion cells (n = 4), with a 4.9 cm^2 diffusion area and compartment volume of 20 mL. The receptor chamber was filled with PBS pH 7.4 and the porcine epithelium was mounted between the acceptor and donor compartments. The 3D printed formulations were carefully attached on the porcine mucosa, followed by instillation of 2 mL SSF. Aliquots (1 mL) were withdrawn from the receptor chamber at 0.5, 1.0, 1.5, 2.0, 4.0 and 6.0 h, centrifuged at 4000 rcf for 20 min and filtered through 0.45 μm polyvinylidene fluoride (PVDF) filters. The receptor chamber was immediately replenished with equal volume of fresh and preheated (37 °C) PBS. At the end of the experiment, the buccal tissue was immersed in 40 mL HPLC mobile phase and sonicated for 30 min, to recover the accumulated amount of drug. Quantification of the API was accomplished by HPLC. The steady-state mass flux (J_{ss}) was determined as the slope of the cumulative mass-time plotted curve (linear fraction). Calculation of the apparent permeability coefficient (P_{app}) was achieved by utilizing equation $P_{app} = J_{ss}/C_d$, where C_d is the initial donor-associated API concentration. The lag time of drug permeation was determined by extrapolation [22]. Alterations on the buccal epithelium architecture after application of the developed 3D printed films was further investigated.

2.9.3. Histological studies

The obtained mucosa was treated with formalin and embedded in paraffin. A hematoxylin–eosin staining of the specimens was accomplished prior to optical microscopy studies in an Olympus CX31 (Olympus, Tokyo, Japan).

2.10. Statistical analysis

All results are presented as mean ± S.D. of at least n = 3 experiments. Statistical significance was indicated ($p < 0.05$) via unpaired Student's *t*-test.

3. Results and discussion

3.1. Preliminary evaluation

A preliminary assessment methodology was conducted in the context of process repeatability on developing uniform buccal dosage forms. Determination of drug content and weight uniformity of the six different formulation types are presented in Table 1. Formulations under the same subgroup with or without EC backing layer exhibited satisfactory weight uniformity, whereas an increased weight deviation was observed with the WAF-formulations. Since the related edible sheets were manually cut to isolate the developed formulations, weight variations were considered an expected drawback.

Fig. 1 shows representative optical images of the formulations in the absence or presence of a backing layer. Comparison of dose variations among the different formulations resulted in a drug content between 8.92 and 9.10 mg (8.01 ± 0.15% for 0C-X and 1C-X, 5.79 ± 0.17% for 0C-EC and 1C-EC, 4.95 ± 0.18% for 0C-WAF and 1C-WAF). Thus, manual repositioning of the building platform (for 0C-WAF and 1C-WAF) or the presence of an additional 3D printed layer (0C-EC and 1C-EC) did not affect deposition of the molten material and the overall performance of the FDM process. Though, the drug loading percentage in each formulation approach was altered, due to addition of either EC or WAF backing layers.

Another important evidence was the yellow-transparent optical characteristics of the 3D printed PVA-based objects. This is indicative of molecular dispersion of the API in the polymer matrix, although a comprehensive conclusion was derived from the physicochemical evaluation. In absence of backing layers, as presented in the optical

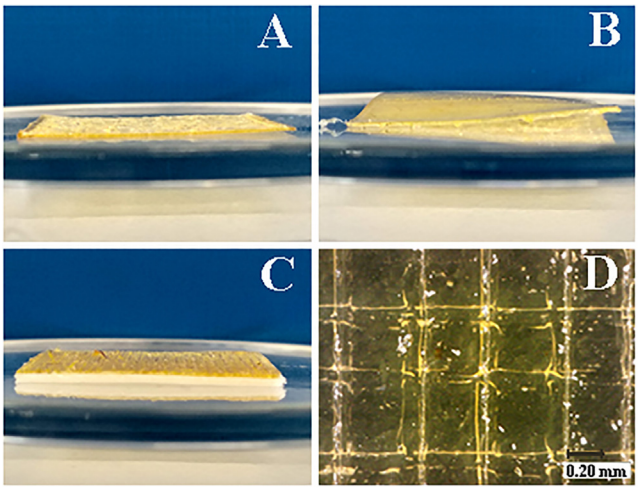

Fig. 1. Representative photos of 3D printed films in the absence (A) and presence of ethyl cellulose (B) or wafer (C) backing layers. (D) Optical micrograph of 0C-X formulations (without chitosan, without backing layer).

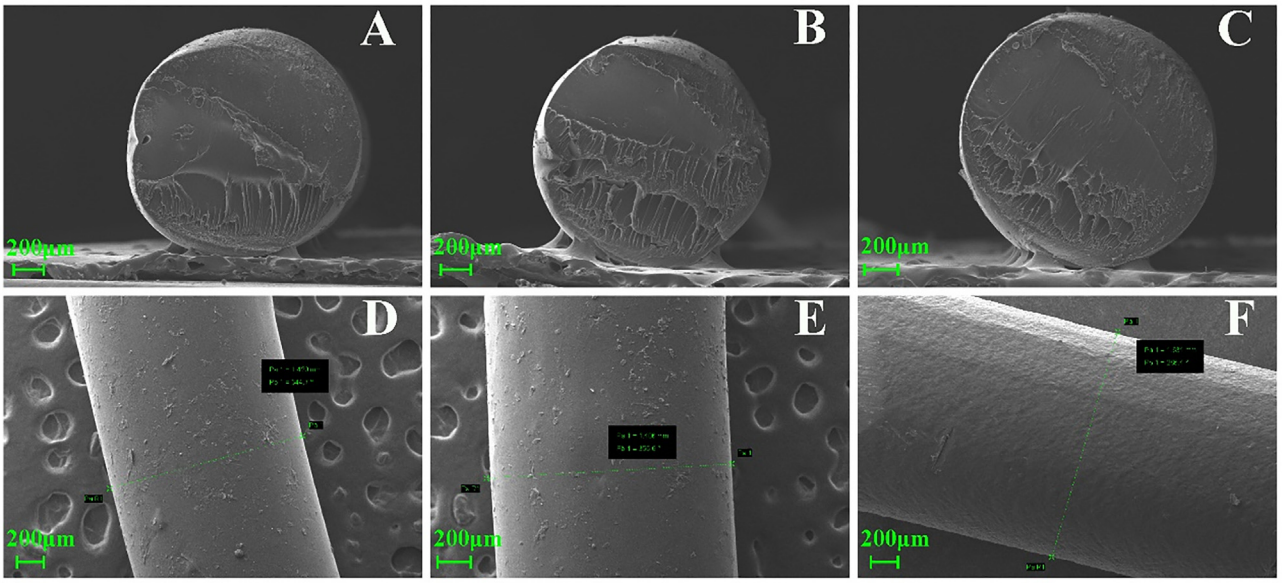

Fig. 2. Micrographs from scanning electron microscopy of PVA filaments without chitosan (A,D), PVA filaments with chitosan (B,E) and ethyl cellulose filaments (C,F).

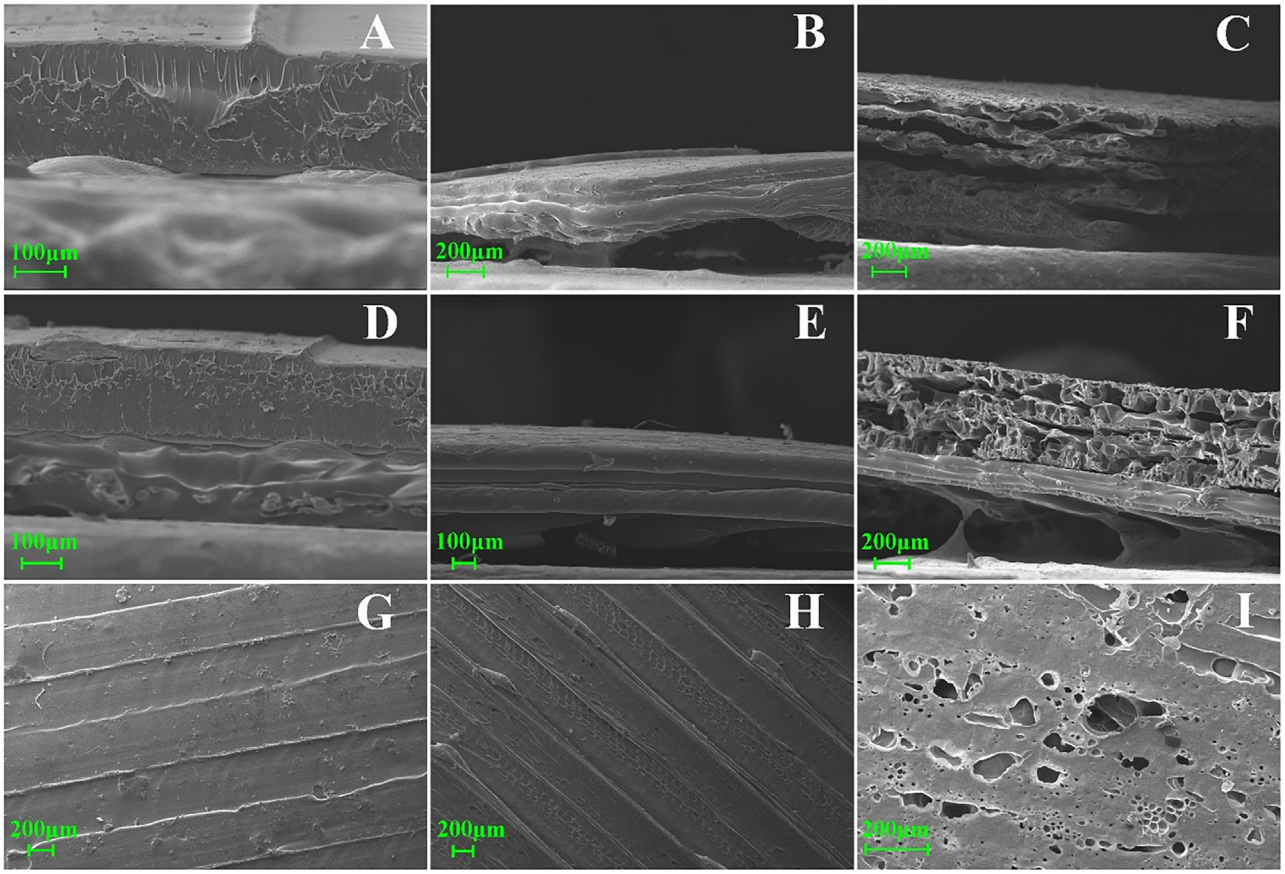

Fig. 3. SEM micrographs of (A) 0C-X, (B) 0C-EC, (C) 0C-WAF, (D) 1C-X, (E) 1C-EC, (F) 1C-WAF formulations. Absence or presence of chitosan is indicated as 0C or 1C. Absence or presence of backing layer is indicated as: X-absence, EC-ethyl cellulose, WAF-wafer. The characteristic pathways generated by the printheads movement on the surface of (G) 0C- or (H) 1C- films. The surface of WAF sheet (I) and the extended porous network.

micrograph in Fig. 1D, transparency of the developed films facilitated imaging of the four consecutive printed layers. These layers were distinguished by crosswise forefront or background stripes, originating from the printhead's motion during the FDM process.

3.2. Physicochemical evaluation

Morphological characteristics of the polymeric filaments, as obtained by SEM, are presented in Fig. 2. Regarding PVA compositions, filament diameters of 1.43 ± 0.03 mm and 1.44 ± 0.03 mm were

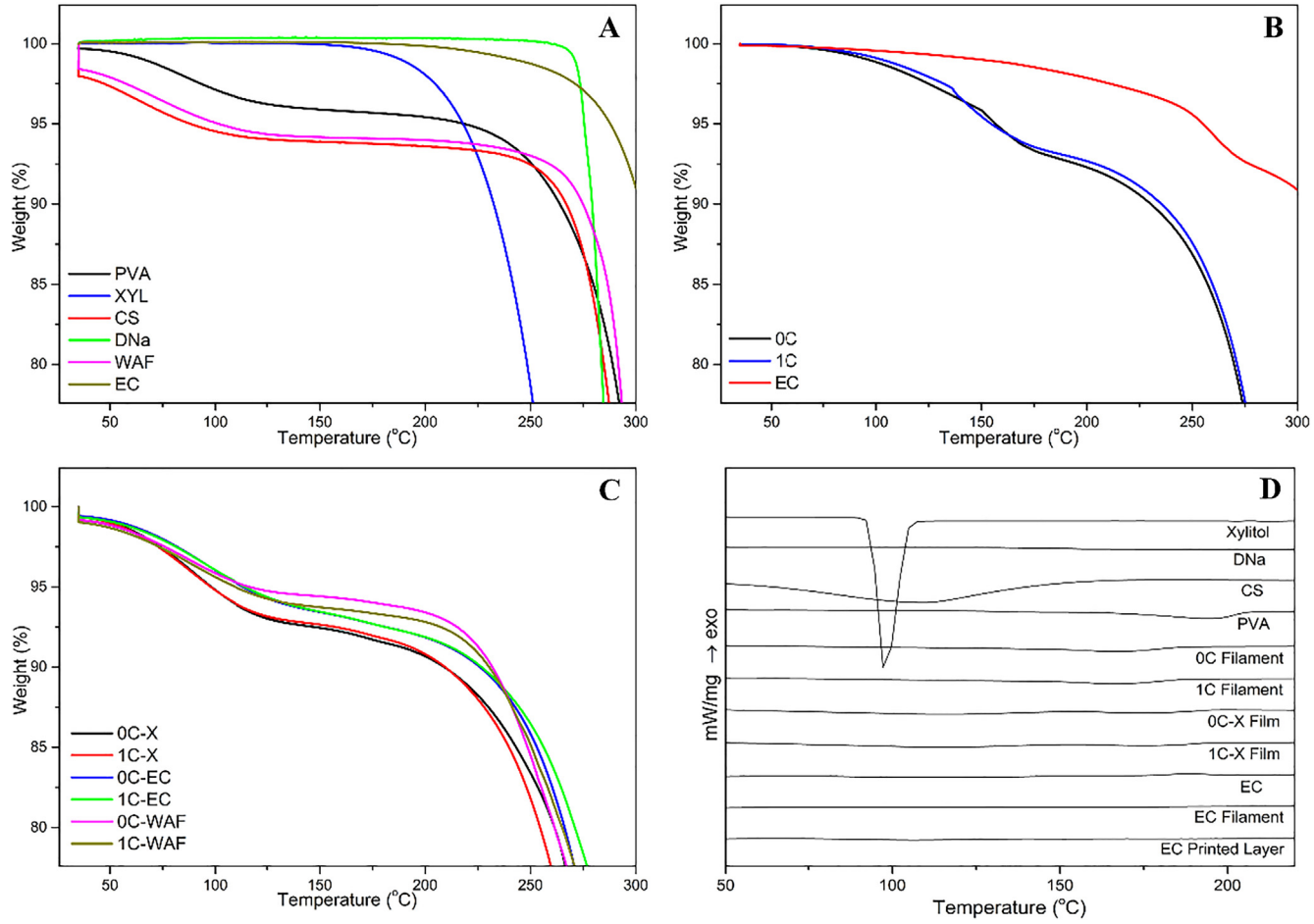

Fig. 4. Thermogravimetric analysis of (A) raw materials (B) filaments and (C) films, with the related differential scanning calorimetry data (D).

Table 2
Extrapolated thermal degradation onset temperatures of raw materials, filaments and films in absence or presence of chitosan (0C, 1C) and absence or presence of a backing layer (X: absence, EC: ethylcellulose, WAF: wafer).

Sample	PVA	Xyl	CS	DNa	EC
T_o [°C]	275	238	243	285	316
Sample	WAF	0C FIlament	1C Filament	EC Filament	0C-X
T_o [°C]	286	261	264	246 / 331	258
Sample	1C-X	0C-EC	1C-EC	0C-WAF	1C-WAF
T_o [°C]	254	252	256	266	267

obtained for 0C and 1C respectively ($p > 0.05$), whereas diameters of 1.64 ± 0.03 mm were acquired for EC filaments. The filament's diameter was adjusted in the 3D printer's software, as indicated by SEM micrographs and manual caliper measurements, to avoid excessive or insufficient extrusion of the molten blend during the printing process. The importance of these observations was reflected on the development of uniform buccal films. Smooth surface and absence of porous internal structure are indicative of homogeneity and consistency of the polymer mixture produced by hot melt extrusion. A smooth external surface of the films was additionally observed for either 0C or 1C formulations, as presented in Fig. 3. Although the different polymer matrices produced distinct clusters in 0C-EC and 1C-EC film structures, successful fusion of the two materials was identified in the interface between the drug loaded compartment and the backing layer (Fig. 3B-E). Satisfactory adhesion between the printed material and edible sheets was further observed in the case of WAF formulations. However, on rare occasions, local detachment of the two compartments was noticed (Fig. 3C), due to inadequate levelling of the platform to consider the layer height of WAF sheets. Moreover, the printhead's movement during the printing process was reflected in representative micrographs of 0C and 1C formulations (Fig. 3G-H), indicating the formation of characteristic pathways with an approximate width of 400 μm, in accordance with the printhead's nozzle diameter. Another important finding was the remarkable porous network extending in the starch-based edible sheet (Fig. 3I).

The TGA and DSC thermograms are illustrated in Fig. 4. The TGA thermograms are presented in the temperature range 35–300 °C, to enhance the clarity of thermal degradation phenomena. The TGA curves of PVA, CS, WAF, PVA-based filaments and 3D printed formulations presented initial weight losses at the temperature range 50–150 °C, attributed to evaporation of water [47]. The extrapolated onset temperatures (T_o) of thermal degradation for all samples are presented in Table 2 (extrapolation not shown). The obtained results indicated safe incorporation of the materials in the applied high-temperature conditions.

The investigated temperature range of DSC studies complied with the extrapolated thermal degradation onset temperatures, as evidenced by TGA measurements (Table 2). DSC results indicated the absence of Xyl endotherm and a remarkable reduction in the melting point of PVA from 195 °C to 165–170 °C for filaments and films, due to complete blending of these compounds and the effective plasticizing effect of xylitol [48]. The melting point of the drug was identified at 281 °C (Fig. S2), followed by the immediate decomposition exotherm [49]. Regarding EC, determination of the glass transition temperature (T_g) was difficult, due to the strong glass forming property of the polymer with weak rheological and heat capacity changes during the transition step,

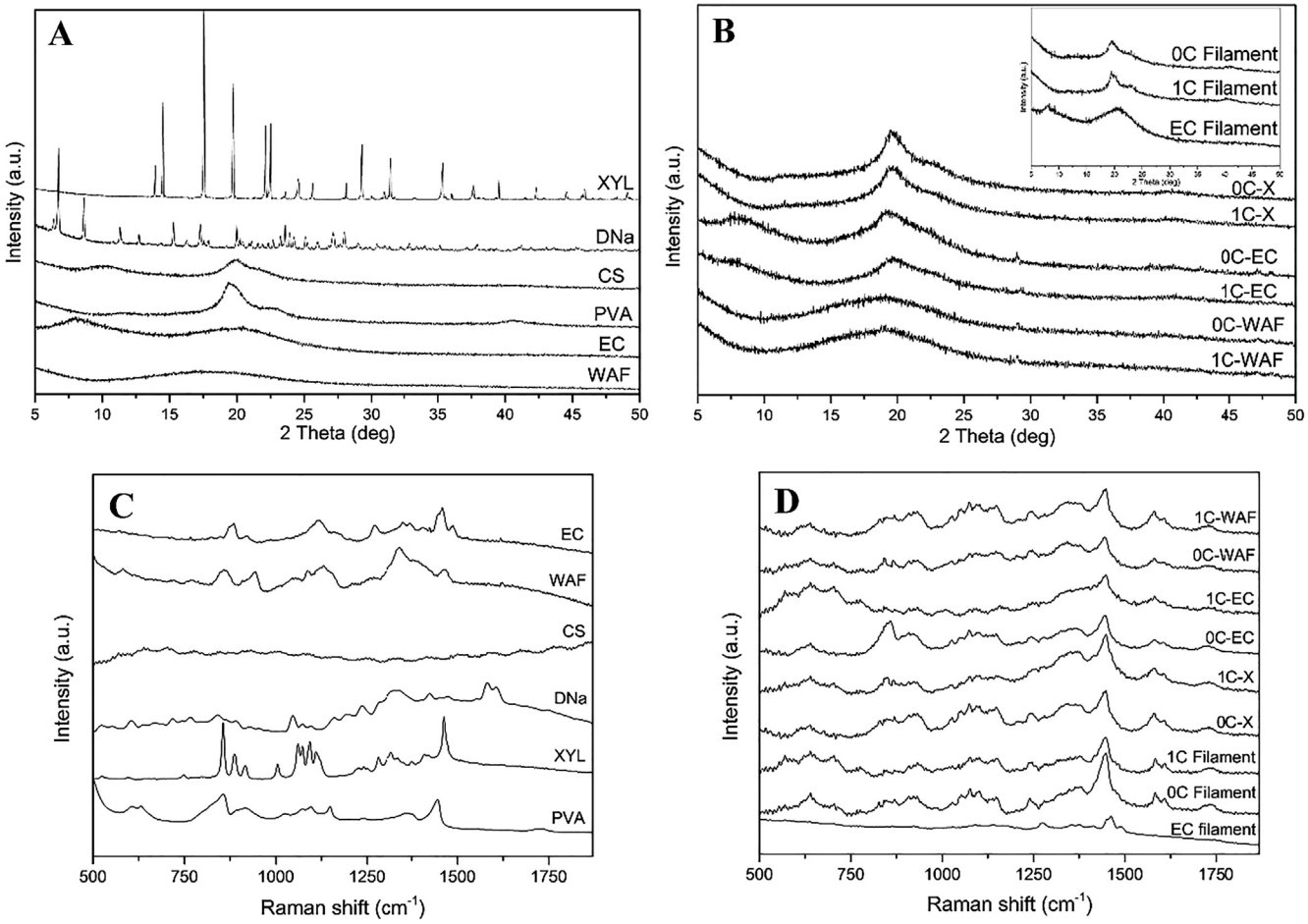

Fig. 5. X-ray diffraction patterns (A and B) and Raman spectra (C and D) of raw materials, filaments and films.

resulting in baseline change [50]. The plasticization effect of TEC was identified by T_g reduction from 112 °C to 105 °C for raw EC and EC filaments/printed-layers respectively. Additionally, a sequence of endo/exothermic events was detected at the region 175–200 °C, ascribed to the polymer's microcrystals melting followed by oxidative degradation [50].

XRPD patterns of raw materials, extruded filaments and printed formulations are presented in Fig. 5A & B. Distinct peaks of Xyl and DNa were observed in the studied 2θ range, indicating their crystalline state. The amorphous state of PVA was identified via a broad amorphous halo centered at around 2θ = 19.4° and a shoulder at 2θ = 22.6°. Moreover, the amorphous halos centered at around 2θ = 20.1°, 2θ = 20.5° and 2θ = 17.4° specified the amorphous state of CS, EC and WAF respectively. The diffractograms of filaments and 3D printed formulations followed the patterns of each incorporated polymer. Regarding the PVA-based products, absence of Xyl peaks evidenced the PVA-Xyl plasticization effect supporting the relevant DSC findings. Furthermore, the DNa characteristic peaks disappeared in both filaments and films, indicating molecular dispersion of the API in the heat-processed polymer matrix during HME and 3D printing, as previously suggested from Fig. 1D. Incorporation of CS in the composition of 1C-filaments and films did not alter the diffraction patterns compared to their 0C-counterparts, suggesting complete blending of CS with PVA. However, incorporation of a backing layer in the developed formulations was reflected in noticeable peak-broadening with subtle 2θ shifts toward the respective diffraction patterns of raw EC or WAF.

Raman spectra (Fig. 5C & D) of pure DNa exhibited characteristics peaks at 1046 cm^{-1} and 1073 cm^{-1}, due to phenylacetate and dichlorophenyl rings breathing vibrations, whereas strong stretching vibrations of the aforementioned rings were additionally observed at 1605 cm^{-1} and 1583 cm^{-1}, respectively [51]. Interpretation of the CS spectrum was not possible, due to a disturbed signal observed over the studied range due to fluorescence of chitosan [52]. The bands of PVA located at 850 cm^{-1} and 909 cm^{-1} were assigned to C—C stretching vibrations. A peak corresponding to C—H bending was additionally identified at 1444 cm^{-1} [53]. Characteristic peaks in the range 800–900 cm^{-1} and 1000–1150 cm^{-1} were evidenced in the spectrum of Xyl, attributed to stretching vibrations of CCO groups [54]. The fluorescent effect of CS was identified in 1C-products (filament/films) via disturbed bands in the range 500–1000 cm^{-1}. Characteristics bands in the range 1000–1150 cm^{-1} and 1480 cm^{-1} indicated vibrations of the respective Xyl and PVA patterns. The presence of DNa was reflected in broad peaks in the range 1550–1610 cm^{-1}; though, the bands of DNa showed a shift to approximately 1603 cm^{-1} and 1580 cm^{-1} in drug loaded films. Similar observations have been peen previously reported with Raman studies on the interactions of DNa with β-cyclodextrin, ammonio methacrylate copolymer and ureasil–poly(ethylene oxide) hybrid matrix [49,51,55]. The authors suggested a plasticizing effect of the drug on the polymer's chains, concluding that broadening and shift of the characteristic bands of DNa are indicative of interactions between the phenylacetate group of DNa and the molecules under investigation.

3.3. Mechanical properties

The resistance of oromucosal preparations to handling-related alterations on the structural characteristics and the overall integrity of the dosage form, is generally referred in the corresponding monograph

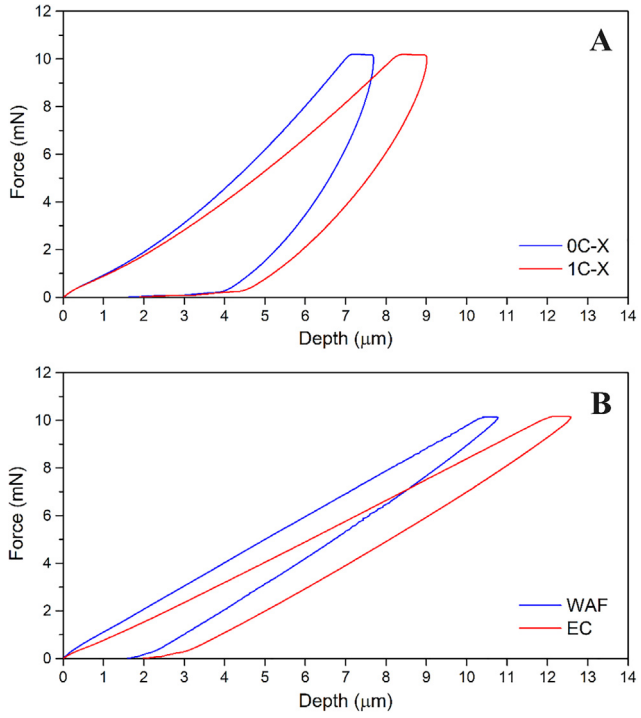

Fig. 6. Typical indentation force-depth curves of (A) formulations without backing layer (X) in presence or absence of chitosan and (B) plain wafer (WAF) sheet and printed ethyl cellulose (EC) layer. Absence or presence of chitosan is indicated as 0C or 1C.

Table 3
Nanoindentation test parameters (Eit: elastic modulus, HV: Vickers hardness) obtained for formulations in absence or presence of chitosan (0C, 1C), plain wafer sheet (WAF) and ethyl cellulose printed layer (EC).

Specimen	Eit [MPa]	HV [MPa]
0C-X	142.78 ± 10.06	0.78 ± 0.05
1C-X	76.85 ± 14.45	0.56 ± 0.06
WAF	54.08 ± 8.57	1.43 ± 0.28
EC	28.05 ± 9.02	0.89 ± 0.03

of Ph.Eur. 8.0 [56]. This prerequisite is expressed via the mechanical strength of the developed formulations; though, specific limitations and definitions are not described in the monograph, regarding a) the appropriate testing method that one should follow to determine the mechanical strength or b) the optimal mechanical properties required for oromucosal dosage forms [56].

In our study, the mechanical properties of 0C-X and 1C-X formulations, along with plain WAF and 3D printed EC-layer, were initially investigated with instrumented indentation tests. Such tests enable local variations of modulus and hardness to be measured precisely [57,58]. The indentation force–depth curves for the four materials under test specified a creep phenomenon at the peak force of 10 mN (Fig. 6). Both WAF and EC have shown smaller creep, while all loading and unloading curves have shown no discontinuities or steps, indicating that no cracks were formed during indentation. The indentation depths at the peak load were identified in the range 7.5–13.0 μm. The 0C-X formulation has shown the lowest indentation depth as compared with the 1C-X film, plain WAF and printed EC materials. Also, the plastic work done was higher for the two formulations 0C-X and 1C-X, as revealed from the increased area enclosed between the loading and unloading curve. In contrary, that behavior was not observed in the loading-unloading response of WAF and EC, indicative of materials that undergo limited plastic deformation. Such results demonstrate the vastly different nature of the materials under study; especially WAF and EC are attached on the 3D printed formulations, and they are not directly comparable with the two different drug loaded compartments, in the context of mechanical properties. The primary use of backing layers is to provide an efficient barrier to drug release from the corresponding surface. The nanoindentation technique can yield precise information on the mechanical performance of the various materials comprising the mucoadhesive buccal films, by measuring their typical bulk properties. This fact is considered beneficial when studying such hybrid systems, intended for pharmaceutical use.

Table 3 shows the results from the indentation test. The elastic modulus of formulation 0C-X was the highest obtained from all tests with a value of 143 MPa. Addition of chitosan for specimens of formulation 1C-X significantly reduced the modulus by approximately 46% to a value of 77 MPa ($p < 0.05$). Similar results were reported in previous studies, as the increase of CS content in PVA/CS blends resulted in significant decrease of the elastic modulus [59]. It was suggested that incorporation of CS in the PVA matrix promoted bond formation between the polymer chains, due to molecular interactions of the PVA- hydroxyl groups and the CS- amine groups. The moduli of plain WAF and EC are even lower with values of 54 MPa and 28 MPa respectively. The hardness measurements though revealed highest values for the WAF sheet (1.43 MPa) followed by the EC layer (0.89 MPa), whereas addition of chitosan in the film composition reduced the measured hardness value from 0.78 MPa to 0.56 MPa for 0C-X and 1C-X formulations respectively ($p < 0.05$), in accordance with the obtained results, regarding the elastic modulus.

To assess the strength of the materials under study, a typical tensile test was performed. The stress-strain curves obtained from the different buccal films are illustrated in Fig. 7A-D. Evidently from Fig. 7(A), the strength of 0C-X formulation was the highest reaching 14 MPa, while for the 1C-X formulation the strength decreased to 10 MPa. The modulus calculated from the elastic part of the stress–strain response is 114 MPa which is around 20% lower than the value obtained via indentation tests. Additionally, the modulus for the 1C-X formulation was calculated as 75.46 MPa which deviated by 2% from the respective value obtained via indentation tests. However, it should be considered that the indentation test measures the performance of the bulk material, while the tensile tests account for the layering structure of the 3D printing operation, as well as the overall geometry of the specimen, i.e. shell and infill, along with any associated printing defects resulting from the 3D printing process. Regarding the strength of the WAF sheet and EC printed layer, as it is shown in Fig. 7B, this was found lower than formulations 0C-X and 1C-X with values of 4.2 MPa and 4.5 MPa respectively. The moduli accounted for 34.6 MPa in the case of EC layer and 68.6 MPa for plain WAF, presenting deviations from the indentation measured values of 22% and 27% respectively. It is interesting to note, as illustrated in Fig. 7C, that a discontinuity step in the stress-strain curve was observed when WAF was incorporated in the formulations. This is rather associated with failure of the wafer sheet at that load, as seen from Fig. 7B, affecting the overall structural integrity of the formulated films. Such observation indicates that the backing layers are undoubtedly different materials, when compared with the drug loaded compartments, in agreement with the results obtained from the indentation tests. In comparison to formulations without a backing layer, significantly lower values were obtained, reaching maximum strength of 7 MPa and 5 MPa for 0C-WAF and 1C-WAF formulations respectively. A marked difference was additionally evidenced in the strength values on 0C-EC and 1C-EC specimens (Fig. 7D), showing lower values compared to 0C-X and 1C-X films. The obtained data were comparable to previous studies related to PVA-based 3D printed films intended for oral delivery of active compounds [17,18].

The flexibility of the developed formulations was further investigated by folding endurance studies. The backing layers presented poor mechanical properties, as also deduced from indentation and tensile tests. Thus, films with either WAF or EC backing layers were folded only one time, due to failure of the backing layer. In the absence

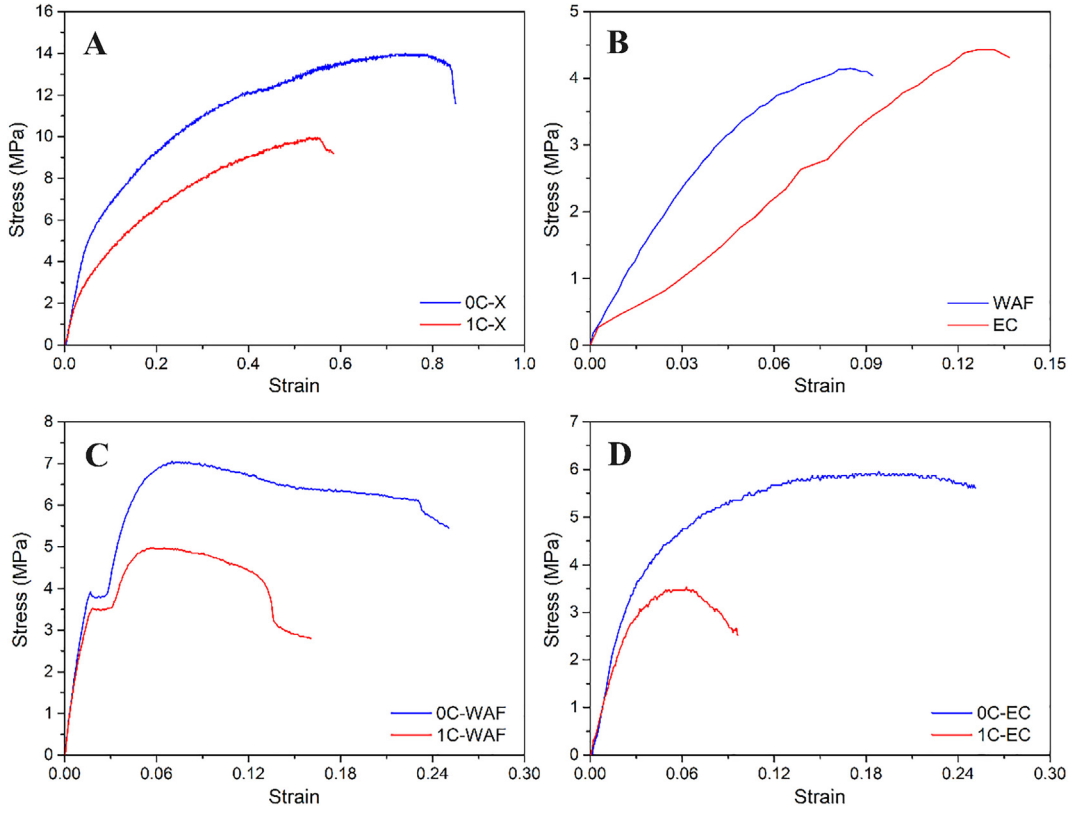

Fig. 7. Typical tensile stress-strain curves of (A) formulations in absence of a backing layer, (B) plain wafer sheet and printed ethyl cellulose layer, (C) formulations in presence of a wafer backing layer, (D) formulations in presence of an ethyl cellulose backing layer. Absence or presence of chitosan is indicated as 0C or 1C. Absence or presence of a backing layer is indicated as: X-absence, EC-ethyl cellulose, WAF-wafer.

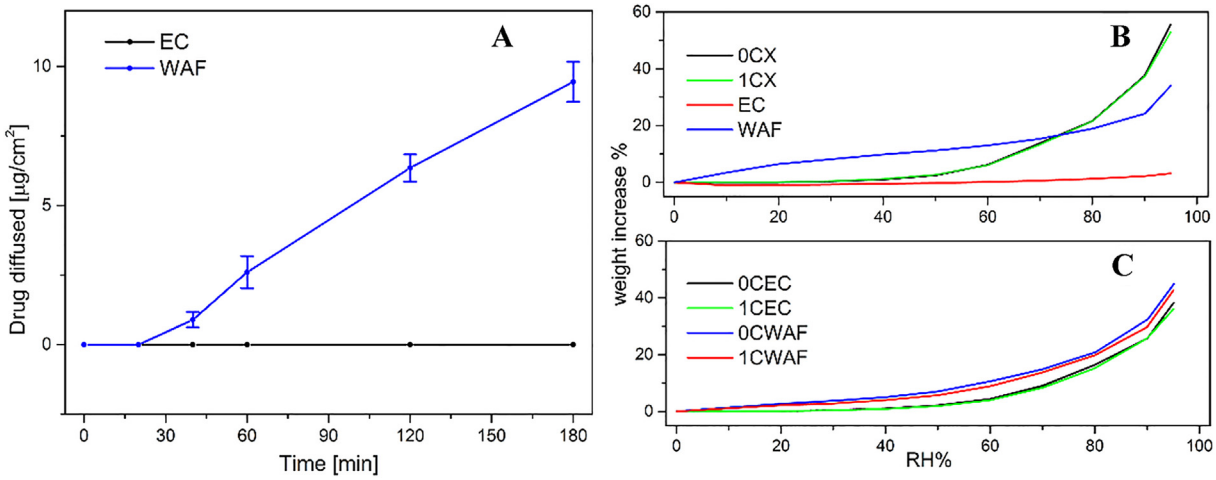

Fig. 8. (A) Drug diffusion across EC (ethyl cellulose) and WAF (wafer) backing layers. (B) Water vapor sorption profiles of plain backing layers and developed films. Absence or presence of chitosan is indicated as 0C or 1C. Absence or presence of a backing layer is indicated as: X-absence, EC-ethyl cellulose, WAF-wafer.

of backing layer, both 0C-X and 1C-X films were folded at a minimum number of 300 times without rupture. High values of folding endurance are indicative of excellent applicability on the administration site, without film dislocation or breaking [60].

3.4. In vitro studies

3.4.1. Evaluation of backing layers

Diffusion of the API throughout the 3D printed EC layer or adjusted WAF sheet was of critical importance, to induce unidirectional properties on the developed formulations. The concept of formulating buccal dosage forms with backing layers is well documented; the backing layer is intended to control the drug release direction, reduce drug loss in the oral cavity and enhance the adhesion time, by acting as a barrier to saliva diffusion into the drug loaded compartment and restricting morphological alterations when applied on the administration site [26]. The diffusion profiles of DNa through the studied materials are presented in Fig. 8A. The hydrophobic EC printed layer prevented diffusion of the API during the experiment. There are several reports in the literature indicating EC as a material of choice to develop impermeable backing layers [61,62]. Incorporation of wafer sheet exhibited limited drug diffusion, with a lag time of 14 min and diffusion

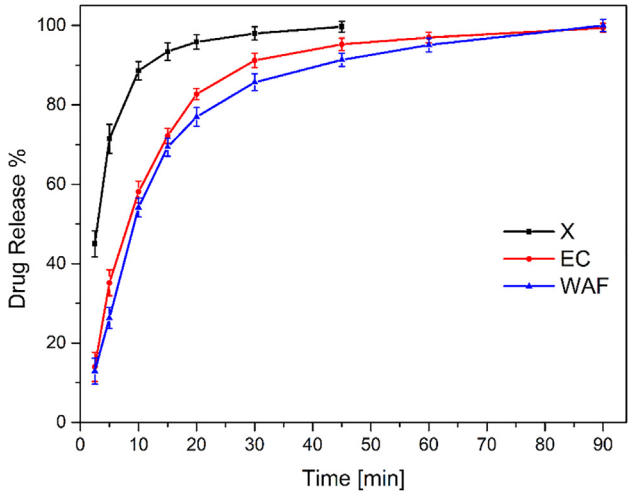

Fig. 9. Drug release profiles of the developed films in simulated saliva. Absence or presence of a backing layer is indicated as: X-absence, EC-ethyl cellulose, WAF-wafer.

Table 4
Fitting parameters for release kinetic models of formulations without backing layer (X) and with ethylcellulose (EC) or wafer (WAF) backing layer.

Backing Layer	First order		Korsmeyer-Peppas			Hixson-Crowell	
	k	R^2	k	n	R^2	k	R^2
X	0.2432	0.9910	–	–	–	0.0345	0.2219
EC	0.0841	0.9953	26.36	0.3241	0.8407	0.0170	0.8687
WAF	0.0712	0.9923	22.39	0.3578	0.8658	0.0165	0.9263

mass flux of 0.058 ± 0.008 μg cm^{-2} min^{-1}. Upon contact of the starch-based material with SSF, development of a gel-like form was induced [63,64], resulting in a structural barrier to drug diffusion.

3.4.2. Water-uptake

Common methods to implement water uptake studies of buccal dosage forms are gravimetrically and dimensionally oriented [44]. These methods incorporate monitoring of the weight/size variations during hydration upon contact of the formulation with simulated biological fluids or specific RH environments. In the absence of a backing layer, rapid deformation of the SSF-hydrated 0C-X and 1C-X formulations rendered this method impractical to produce meaningful data, due to inconvenient manual handling of the films. Thus, the vapor sorption methodology was followed in the current study.

Fig. 8B & C illustrate the effects of formulation characteristics on the absorption performance of buccal films. Significant observations were depicted in the presence of a backing layer, although the CS content did not induce alterations in the degree of hydration. Formulations 0C- and 1C-X indicated a vapor sorption capacity of 56% and 53% respectively, while plain WAF presented a weight gain of 34.1% at RH 95%. Contrariwise, at RH conditions up to 70%, a remarkably higher vapor sorption capacity of WAF was evidenced, compared to 0C- and 1C-X films. This finding is indicative of the large porous network existing in the starch-based matrix (Fig. 3I). An expected result was the negligible amount of water maximally absorbed in the case of EC printed layer (3.2%), due to the hydrophobic nature of the polymer. Regarding the presence of backing layer, EC and WAF formulations exhibited a reduced amount of absorbed water, 36.0–38.2% and 42.5–44.8% respectively, associated with the corresponding degree of hydration of plain EC and WAF materials.

3.4.3. Release studies

An array of methods for conducting release studies on oromucosal preparations, are reported in the literature with media volumes up to 1000 mL [30,33,65–68]. However, complete immersion of the fabricated films in the medium could not be achieved with limited volumes of SSF. Positioning the formulation on a horizontal plane over the release chamber, was considered inefficient to discriminate variations in the release behavior, relevant to the presence/type of backing layers. Thus, a volume of 50 mL was selected in our study, to maintain the films completely immersed in the SSF-containing chamber.

The release studies, carried out in SSF, were grouped by type of backing layer, since incorporation of CS did not induce any variations between the performance of 0C- and 1C-films ($p > 0.05$). The corresponding release profiles are illustrated in Fig. 9. A significant burst release was noticed only in the case of 3D printed films without a backing layer (X), as approximately 45% ($p < 0.05$) of the API content was released in 2.5 min, whereas after incorporation of EC- and WAF-backing layers the respective values were determined at 14% and 13%. A DNa amount of 90% was released within 20 min for X-films, 30 min for EC-films and 45 min for WAF-films. Complete release of the drug was implemented within 45 min for X-formulations, whereas the release process was extended up to 90 min in the presence of a backing layer. In the case of X-films, the hydrophilicity of PVA, combined with exposure of both external surfaces of the formulation to SSF, resulted in a burst release effect. Investigation of the different backing layers presented similar initial behavior for 15 min. Incorporation of EC or WAF backing layers generated an effective barrier to SSF diffusion in the drug loaded compartment, thus facilitating unidirectional release

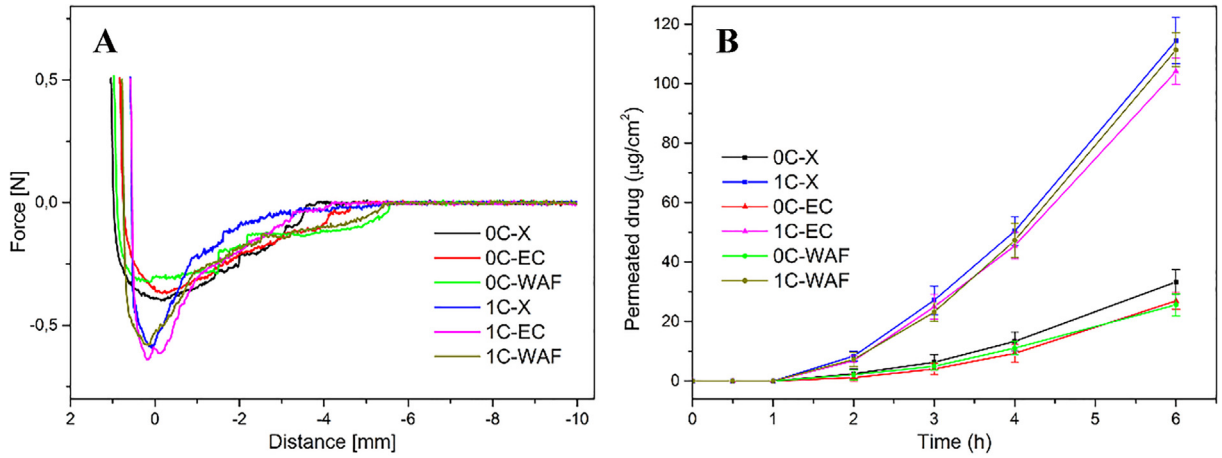

Fig. 10. (A) Mucoadhesion profiles of the developed formulations and (B) Drug permeation across porcine buccal epithelium. Absence or presence of chitosan is indicated as 0C or 1C. Absence or presence of a backing layer is indicated as: X-absence, EC-ethyl cellulose, WAF-wafer.

Table 5
Steady state fluxes (J_{ss}) and apparent permeability coefficients (P_{app}) of 3D printed films with (1C) or without (0C) chitosan and with or without a backing layer (X: absence, EC: ethylcellulose, WAF: wafer) across porcine buccal epithelium (n = 4 ± S.D.).

Formulation	J_{ss} [μg cm^{-2} h^{-1}]	$P_{app}10^3$ [cm h^{-1}]	Lag time [h]	Extracted [mg]
0C-X	8.24 ± 0.56	1.83 ± 0.17	2.14 ± 0.03	0.53 ± 0.08
1C-X	27.64 ± 0.42	6.14 ± 0.14	1.90 ± 0.04	2.70 ± 0.10
0C-EC	6.52 ± 0.95	1.45 ± 0.21	2.18 ± 0.17	0.49 ± 0.06
1C-EC	24.33 ± 0.73	5.41 ± 0.24	1.88 ± 0.05	2.57 ± 0.15
0C-WAF	6.86 ± 0.97	1.57 ± 0.28	2.14 ± 0.19	0.52 ± 0.10
1C-WAF	24.71 ± 0.61	5.55 ± 0.36	1.91 ± 0.07	2.50 ± 0.18

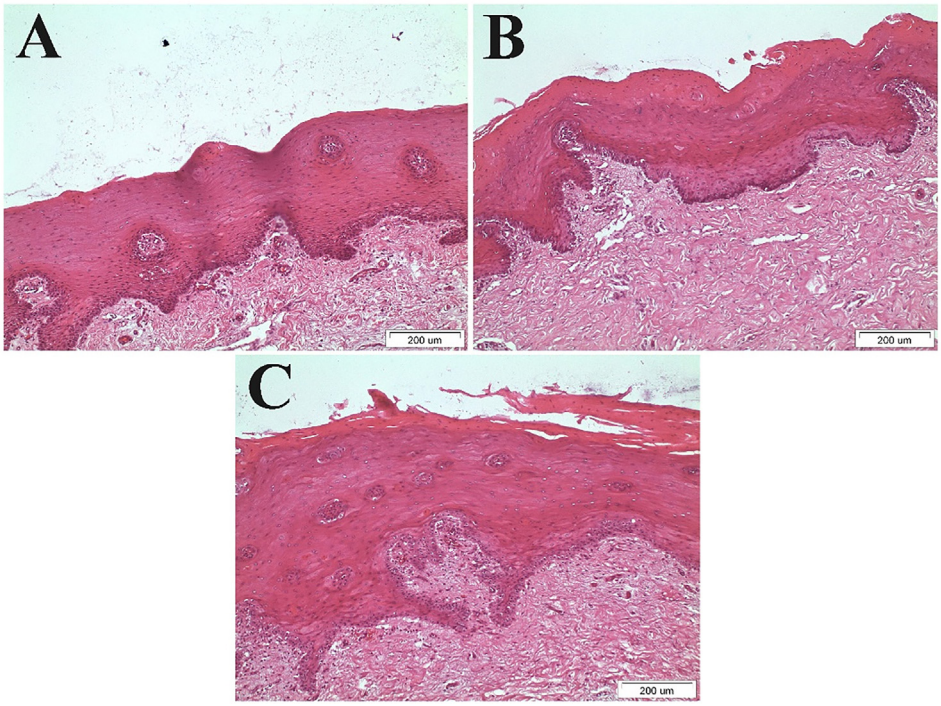

Fig. 11. Microscopic appearance of porcine buccal mucosa after 6 h of permeation studies (A) control, (B) film without chitosan, (C) film with chitosan.

and reduced release rate compared to the X-counterparts. However, variations in the release profiles were observed at 20 min. An appreciable amount of the drug migrated and entrapped into the gel matrix formed after hydration of the starch-based material, which additionally acted as a release retardant. These data were further fitted in three kinetic models and presented in Table 4. The Korsmeyer-Peppas equation was excluded from fitting on the X-films obtained data, since these formulations exhibited significant burst release profiles [69]. All formulations exhibited optimal fitting in first order kinetics, with R^2 values in the range 0.9910–0.9953. According to the kinetic theory of the model, the profiles demonstrate a constantly decreasing release rate, which is highly dependent to the remaining drug in the dosage form [69].

3.5. Ex vivo evaluation

3.5.1. Mucoadhesion of films

Investigation of the CS effect on the mucoadhesive properties of buccal formulations was carried out after applying the 0C- and 1C-films (in the presence or absence of a backing layer) on porcine buccal mucosa. Representative mucoadhesion profiles of the different dosage forms are illustrated in Fig. 10A. The presence and the type of a backing layer is expected to act as a water diffusion barrier toward the drug loaded compartment, thus affecting the mucoadhesive performance of buccal dosage forms [26]. However, in the current *ex-vivo* experimentation, only a small amount of SSF was in direct contact with the drug loaded compartment, while the backing layer was attached to the instrument's probe. As expected, comparison of the 3D printed formulations regarding the backing layer type resulted in insignificant variations ($p > 0.05$). Therefore, the calculated mucoadhesion parameters where categorized by CS content. The W_{ad} and DF_{max} values for 0C-films were calculated at 1.490 ± 0.298 Nm and 0.378 ± 0.039 N respectively, ascribed to the mucoadhesive properties of PVA [70,71]. The obtained data further reflected the impact of CS content in the dosage form composition. A significant increase of DF_{max} by 52% and W_{ad} by 40% indicated the positive effect of CS as mucoadhesion enhancer [72,73], thus attributing an additional mucoadhesive effect to the PVA-based films ($p < 0.05$). In general, the 3D printed 0C- and 1C-formulations exhibited comparable mucoadhesive performance to previous studies, reporting PVA- and/or CS-containing buccal dosage forms developed by alternative processes [35,74–76].

3.5.2. Permeation and histological studies

Permeation studies were performed across porcine buccal mucosa, due to morphological similarities with the respective human epithelium. Permeation profiles acquired from the different designs are illustrated in Fig. 10B. Analysis of the data was carried out to determine the permeation parameters and investigate the effects of CS content and structural characteristics on the *ex vivo* performance of 3D printed formulations. Significant alterations on the profiles were observed ($p < 0.05$), when 0C- and 1C-films were compared, as presented in Table 5. In absence of CS, the steady state flux and the apparent

permeability coefficient were determined in the range 6.524–8.241 μg cm^{-2} h^{-1} and 1.346–1.831 cm h^{-1}, respectively. Incorporation of CS in the composition of PVA-based formulations contributed to higher mass transfer throughout the epithelium, exhibiting a more than threefold increase in permeation parameters for either X-, EC- or WAF-films ($p < 0.05$). Moreover, a 10.7–13.8% reduction in lag time was evidenced in all cases. A remarkable effect of CS was indicated after quantification of the tissue-extracted API. The amount of extracted DNa from buccal tissues was in the range 0.49–0.53 mg for 0C-formulations, whereas for CS-incorporating films the drug recovery accounted to 2.50–2.70 mg ($p < 0.05$). This finding is indicative of the cationic-CS interaction with the buccal membrane which results in reorganization of the tight protein junctions [77]. The CS permeation enhancement effect was further reflected on the micrographs in Fig. 11.

Histological assessment of the buccal epithelium revealed moderate desquamation after application of the PVA-based formulations (Fig. 11B), compared to the control tissue (Fig. 11A). As Fig. 11C reveals, application of the 1C-films induced stronger superficial desquamation, with local epithelium detachment. The obtained permeation parameters are comparable with previous *ex vivo* studies, reporting the effect of DNa ionization from bioadhesive hydrophilic matrices on porcine buccal permeation [78]. On the contrary, increased values of DNa transport have also been reported across chicken buccal epithelium [79], suggesting that variations on *ex vivo* performance are generated from the type/origin of the membrane [78].

4. Conclusions

In our work, the use of additive manufacturing by FDM 3D printing for buccal films was investigated. The manufactured products exhibited acceptable structural features and dose uniformity. The solid-state characterization indicated effective plasticization of the polymer, complete blending of the integrated components, and amorphization of the drug. The obtained mechanical properties evidenced alterations on the performance of films in nanoindentation and tensile tests, either when chitosan was incorporated in the formulation composition or after addition of a backing layer. Unidirectional release of the active component, acceptable vapor sorption properties and modified release profiles, associated with the presence and type of backing layer, were evidenced by *in vitro* evaluations. The presence of chitosan affected the *ex vivo* performance of formulated films, demonstrating enhanced mucoadhesion and permeation properties. The overall study confirmed the hypothesis of 3D printing exploitation toward fabrication of oromucosal buccal dosage forms.

Acknowledgements

This research is co-financed by Greece and the European Union (European Social Fund- ESF) through the Operational Programme «Human Resources Development, Education and Lifelong Learning» in the context of the project “Strengthening Human Resources Research Potential via Doctorate Research” (MIS-5000432), implemented by the State Scholarships Foundation (ΙΚΥ). This research has also received financing from NordForsk, the Nordic University Hub project #85352 (Nordic POP, Patient Oriented Products).

Appendix A. Supplementary material

Supplementary data to this article can be found online at https://doi.org/10.1016/j.ejpb.2019.09.018.

References

[1] M. Preis, J. Breitkreutz, N. Sandler, Perspective: Concepts of printing technologies for oral film formulations, Int. J. Pharm. 494 (2015) 578–584.
[2] B. Arafat, N. Qinna, M. Cieszynska, R.T. Forbes, M.A. Alhnan, Tailored on demand anti-coagulant dosing: An in vitro and in vivo evaluation of 3D printed purpose-designed oral dosage forms, Eur. J. Pharm. Biopharm. 128 (2018) 282–289.
[3] C.I. Gioumouxouzis, C. Karavasili, D.G. Fatouros, Recent advances in pharmaceutical dosage forms and devices using additive manufacturing technologies, Drug Discov. Today. 24 (2018) 636–643.
[4] M. Alhijjaj, P. Belton, S. Qi, An investigation into the use of polymer blends to improve the printability of and regulate drug release from pharmaceutical solid dispersions prepared via fused deposition modeling (FDM) 3D printing, Eur. J. Pharm. Biopharm. 108 (2016) 111–125.
[5] K. Pietrzak, A. Isreb, M.A. Alhnan, A flexible-dose dispenser for immediate and extended release 3D printed tablets, Eur. J. Pharm. Biopharm. 96 (2015) 380–387.
[6] A. Goyanes, A.B.M. Buanz, G.B. Hatton, S. Gaisford, A.W. Basit, 3D printing of modified-release aminosalicylate (4-ASA and 5-ASA) tablets, Eur. J. Pharm. Biopharm. 89 (2015) 157–162.
[7] A. Goyanes, J. Wang, A. Buanz, R. Martínez-Pacheco, R. Telford, S. Gaisford, A.W. Basit, 3D Printing of medicines: engineering novel oral devices with unique design and drug release characteristics, Mol. Pharm. 12 (2015) 4077–4084.
[8] M. Sadia, B. Arafat, W. Ahmed, R.T. Forbes, M.A. Alhnan, Channelled tablets: An innovative approach to accelerating drug release from 3D printed tablets, J. Controlled Release. 269 (2018) 355–363.
[9] G. Verstraete, A. Samaro, W. Grymonpré, V. Vanhoorne, B. Van Snick, M.N. Boone, T. Hellemans, L. Van Hoorebeke, J.P. Remon, C. Vervaet, 3D printing of high drug loaded dosage forms using thermoplastic polyurethanes, Int. J. Pharm. 536 (2018) 318–325.
[10] C.I. Gioumouxouzis, O.L. Katsamenis, N. Bouropoulos, D.G. Fatouros, 3D printed oral solid dosage forms containing hydrochlorothiazide for controlled drug delivery, J. Drug Deliv. Sci. Technol. 40 (2017) 164–171.
[11] T.C. Okwuosa, B.C. Pereira, B. Arafat, M. Cieszynska, A. Isreb, M.A. Alhnan, Fabricating a shell-core delayed release tablet using dual FDM 3D printing for patient-centred therapy, Pharm. Res. 34 (2017) 427–437.
[12] X. Chai, H. Chai, X. Wang, J. Yang, J. Li, Y. Zhao, W. Cai, T. Tao, X. Xiang, Fused deposition modeling (FDM) 3D printed tablets for intragastric floating delivery of domperidone, Sci. Rep. 7 (2017).
[13] C.I. Gioumouxouzis, A.-T. Chatzitaki, C. Karavasili, O.L. Katsamenis, D. Tzetzis, E. Mystiridou, N. Bouropoulos, D.G. Fatouros, Controlled release of 5-fluorouracil from alginate beads encapsulated in 3D printed ph-responsive solid dosage forms, AAPS PharmSciTech. 19 (2018) 3362–3375.
[14] A. Maroni, A. Melocchi, F. Parietti, A. Foppoli, L. Zema, A. Gazzaniga, 3D printed multi-compartment capsular devices for two-pulse oral drug delivery, J. Controlled Release. 268 (2017) 10–18.
[15] R.C.R. Beck, P.S. Chaves, A. Goyanes, B. Vukosavljevic, A. Buanz, M. Windbergs, A.W. Basit, S. Gaisford, 3D printed tablets loaded with polymeric nanocapsules: An innovative approach to produce customized drug delivery systems, Int. J. Pharm. 528 (2017) 268–279.
[16] D. Markl, J.A. Zeitler, C. Rasch, M.H. Michaelsen, A. Müllertz, J. Rantanen, T. Rades, J. Bøtker, Analysis of 3D prints by X-ray computed microtomography and terahertz pulsed imaging, Pharm. Res. 34 (2017) 1037–1052.
[17] W. Jamróz, M. Kurek, E. Łyszczarz, J. Szafraniec, J. Knapik-Kowalczuk, K. Syrek, M. Paluch, R. Jachowicz, 3D printed orodispersible films with Aripiprazole, Int. J. Pharm. 533 (2017) 413–420.
[18] T. Ehtezazi, M. Algellay, Y. Islam, M. Roberts, N.M. Dempster, S.D. Sarker, The application of 3D printing in the formulation of multilayered fast dissolving oral films, J. Pharm. Sci. 107 (2018) 1076–1085.
[19] K. Liang, S. Carmone, D. Brambilla, J.-C. Leroux, 3D printing of a wearable personalized oral delivery device: A first-in-human study, Sci. Adv. 4 (2018) eaat2544.
[20] J.O. Morales, J.T. McConville, Manufacture and characterization of mucoadhesive buccal films, Eur. J. Pharm. Biopharm. 77 (2011) 187–199.
[21] U.D. Kulkarni, R. Mahalingam, X. Li, I. Pather, B. Jasti, Effect of experimental temperature on the permeation of model diffusants across porcine buccal mucosa, AAPS PharmSciTech. 12 (2011) 579–586.
[22] S.E. Hansen, E. Marxen, C. Janfelt, J. Jacobsen, Buccal delivery of small molecules – Impact of levulinic acid, oleic acid, sodium dodecyl sulfate and hypotonicity on ex vivo permeability and spatial distribution in mucosa, Eur. J. Pharm. Biopharm. 133 (2018) 250–257.
[23] A. Kokate, X. Li, B. Jasti, Effect of drug lipophilicity and ionization on permeability across the buccal mucosa: a technical note, AAPS PharmSciTech. 9 (2008) 501–504.
[24] C. Padula, S. Pescina, S. Nicoli, P. Santi, New insights on the mechanism of fatty acids as buccal permeation enhancers, Pharmaceutics. 10 (2018) 201.
[25] J.A. Nicolazzo, B.L. Reed, B.C. Finnin, Buccal penetration enhancers—How do they really work? J. Controlled Release. 105 (2005) 1–15.
[26] N. Salamatmiller, M. Chittchang, T. Johnston, The use of mucoadhesive polymers in buccal drug delivery, Adv. Drug Deliv. Rev. 57 (2005) 1666–1691.
[27] J. Smart, The basics and underlying mechanisms of mucoadhesion, Adv. Drug Deliv. Rev. 57 (2005) 1556–1568.
[28] R. Kolakovic, T. Viitala, P. Ihalainen, N. Genina, J. Peltonen, N. Sandler, Printing technologies in fabrication of drug delivery systems, Expert Opin. Drug Deliv. 10 (2013) 1711–1723.
[29] D. Vetchý, H. Landová, J. Gajdziok, P. Doležel, Z. Daněk, J. Štembírek, Determination of dependencies among in vitro and in vivo properties of prepared mucoadhesive buccal films using multivariate data analysis, Eur. J. Pharm. Biopharm. 86 (2014) 498–506.
[30] R. Trastullo, A. Abruzzo, B. Saladini, M.C. Gallucci, T. Cerchiara, B. Luppi, F. Bigucci, Design and evaluation of buccal films as paediatric dosage form for transmucosal delivery of ondansetron, Eur. J. Pharm. Biopharm. 105 (2016) 115–121.
[31] P. Paolicelli, S. Petralito, G. Varani, M. Nardoni, S. Pacelli, L. Di Muzio, J. Tirillò,

C. Bartuli, S. Cesa, M.A. Casadei, A. Adrover, Effect of glycerol on the physical and mechanical properties of thin gellan gum films for oral drug delivery, Int. J. Pharm. 547 (2018) 226–234.
[32] R.O. do Couto, C. Cubayachi, P.L. Calefi, R.F.V. Lopez, V. Pedrazzi, C.M. De Gaitani, O. de Freitas, Combining amino amide salts in mucoadhesive films enhances needle-free buccal anesthesia in adults, J. Controlled Release 266 (2017) 205–215.
[33] M. Preis, C. Woertz, K. Schneider, J. Kukawka, J. Broscheit, N. Roewer, J. Breitkreutz, Design and evaluation of bilayered buccal film preparations for local administration of lidocaine hydrochloride, Eur. J. Pharm. Biopharm. 86 (2014) 552–561.
[34] J. Mašek, D. Lubasová, R. Lukáč, P. Turánek-Knotigová, P. Kulich, J. Plocková, E. Mašková, L. Procházka, Š. Koudelka, N. Sasithorn, J. Gombos, E. Bartheldyová, F. Hubatka, M. Raška, A.D. Miller, J. Turánek, Multi-layered nanofibrous mucoadhesive films for buccal and sublingual administration of drug-delivery and vaccination nanoparticles - important step towards effective mucosal vaccines, J. Controlled Release. 249 (2017) 183–195.
[35] A. Abruzzo, F.P. Nicoletta, F. Dalena, T. Cerchiara, B. Luppi, F. Bigucci, Bilayered buccal films as child-appropriate dosage form for systemic administration of propranolol, Int. J. Pharm. 531 (2017) 257–265.
[36] M.B. Pimparade, A. Vo, A.S. Maurya, J. Bae, J.T. Morott, X. Feng, D.W. Kim, V.I. Kulkarni, R. Tiwari, K. Vanaja, R. Murthy, H.N. Shivakumar, D. Neupane, S.R. Mishra, S.N. Murthy, M.A. Repka, Development and evaluation of an oral fast disintegrating anti-allergic film using hot-melt extrusion technology, Eur. J. Pharm. Biopharm. 119 (2017) 81–90.
[37] I. Speer, M. Preis, J. Breitkreutz, Prolonged drug release properties for orodispersible films by combining hot-melt extrusion and solvent casting methods, Eur. J. Pharm. Biopharm. 129 (2018) 66–73.
[38] A.M. Bhagurkar, M. Darji, P. Lakhani, P. Thipsay, S. Bandari, M.A. Repka, Effects of formulation composition on the characteristics of mucoadhesive films prepared by hot-melt extrusion technology, J. Pharm. Pharmacol. 71 (2019) 293–305.
[39] A. Melocchi, F. Parietti, A. Maroni, A. Foppoli, A. Gazzaniga, L. Zema, Hot-melt extruded filaments based on pharmaceutical grade polymers for 3D printing by fused deposition modeling, Int. J. Pharm. 509 (2016) 255–263.
[40] C.I. Gioumouxouzis, A. Baklavaridis, O.L. Katsamenis, C.K. Markopoulou, N. Bouropoulos, D. Tzetzis, D.G. Fatouros, A 3D printed bilayer oral solid dosage form combining metformin for prolonged and glimepiride for immediate drug delivery, Eur. J. Pharm. Sci. 120 (2018) 40–52.
[41] J. Zhang, X. Feng, H. Patil, R.V. Tiwari, M.A. Repka, Coupling 3D printing with hot-melt extrusion to produce controlled-release tablets, Int. J. Pharm. 519 (2017) 186–197.
[42] Z.C. Kennedy, J.F. Christ, K.A. Evans, B.W. Arey, L.E. Sweet, M.G. Warner, R.L. Erikson, C.A. Barrett, 3D-printed poly(vinylidene fluoride)/carbon nanotube composites as a tunable, low-cost chemical vapour sensing platform, Nanoscale. 9 (2017) 5458–5466.
[43] G.K. Eleftheriadis, P.K. Monou, N. Bouropoulos, D.G. Fatouros, In vitro evaluation of 2D-printed edible films for the buccal delivery of diclofenac sodium, Materials. 11 (2018) 864.
[44] A.B. Nair, R. Kumria, S. Harsha, M. Attimarad, B.E. Al-Dhubiab, I.A. Alhaider, In vitro techniques to evaluate buccal films, J. Controlled Release. 166 (2013) 10–21.
[45] M.R.C. Marques, R. Loebenberg, M. Almukainzi, Simulated biological fluids with possible application in dissolution testing, Dissolution Technol. 18 (2011) 15–28.
[46] M. Guhmann, M. Preis, F. Gerber, N. Pöllinger, J. Breitkreutz, W. Weitschies, Development of oral taste masked diclofenac formulations using a taste sensing system, Int. J. Pharm. 438 (2012) 81–90.
[47] S. Kumar, B. Krishnakumar, A.J.F.N. Sobral, J. Koh, Bio-based (chitosan/PVA/ZnO) nanocomposites film: Thermally stable and photoluminescence material for removal of organic dye, Carbohydr. Polym. 205 (2019) 559–564.
[48] A.A. Aydın, V. Ilberg, Effect of different polyol-based plasticizers on thermal properties of polyvinyl alcohol:starch blends, Carbohydr. Polym. 136 (2016) 441–448.
[49] P. Sipos, M. Szűcs, A. Szabó, I. Erős, P. Szabó-Révész, An assessment of the interactions between diclofenac sodium and ammonio methacrylate copolymer using thermal analysis and Raman spectroscopy, J. Pharm. Biomed. Anal. 46 (2008) 288–294.
[50] H.L. Lai, K. Pitt, D.Q.M. Craig, Characterisation of the thermal properties of ethylcellulose using differential scanning and quasi-isothermal calorimetric approaches, Int. J. Pharm. 386 (2010) 178–184.
[51] T. Iliescu, M. Baia, V. Miclăuş, A Raman spectroscopic study of the diclofenac sodium–β-cyclodextrin interaction, Eur. J. Pharm. Sci. 22 (2004) 487–495.
[52] M. Donmez, H.A. Oktem, M.D. Yilmaz, Ratiometric fluorescence detection of an anthrax biomarker with Eu 3+ -chelated chitosan biopolymers, Carbohydr. Polym. 180 (2018) 226–230.
[53] M. Hema, S. Selvasekarapandian, G. Hirankumar, A. Sakunthala, D. Arunkumar, H. Nithya, Laser Raman and ac impedance spectroscopic studies of PVA: NH4NO3 polymer electrolyte, Spectrochim. Acta. A. Mol. Biomol. Spectrosc. 75 (2010) 474–478.
[54] M. de Veij, P. Vandenabeele, T. De Beer, J.P. Remon, L. Moens, Reference database of Raman spectra of pharmaceutical excipients, J. Raman Spectrosc. 40 (2009) 297–307.
[55] L. Lopes, E.F. Molina, L.A. Chiavacci, C.V. Santilli, V. Briois, S.H. Pulcinelli, Drug–matrix interaction of sodium diclofenac incorporated into ureasil–poly (ethylene oxide) hybrid materials, RSC Adv. 2 (2012) 5629.
[56] R. Krampe, J.C. Visser, H.W. Frijlink, J. Breitkreutz, H.J. Woerdenbag, M. Preis, Oromucosal film preparations: points to consider for patient centricity and manufacturing processes, Expert Opin. Drug Deliv. 13 (2016) 493–506.
[57] D. Tzetzis, G. Mansour, I. Tsiafis, E. Pavlidou, Nanoindentation measurements of fumed silica epoxy reinforced nanocomposites, J. Reinf. Plast. Compos. 32 (2013) 160–173.
[58] G. Mansour, D. Tzetzis, Nanomechanical characterization of hybrid multiwall carbon nanotube and fumed silica epoxy nanocomposites, Polym.-Plast. Technol. Eng. 52 (2013) 1054–1062.
[59] J. Bonilla, E. Fortunati, L. Atarés, A. Chiralt, J.M. Kenny, Physical, structural and antimicrobial properties of poly vinyl alcohol–chitosan biodegradable films, Food Hydrocoll. 35 (2014) 463–470.
[60] G. Tejada, G.N. Piccirilli, M. Sortino, C.J. Salomón, M.C. Lamas, D. Leonardi, Formulation and in-vitro efficacy of antifungal mucoadhesive polymeric matrices for the delivery of miconazole nitrate, Mater. Sci. Eng. C. 79 (2017) 140–150.
[61] A.M. Avachat, K.N. Gujar, K.V. Wagh, Development and evaluation of tamarind seed xyloglucan-based mucoadhesive buccal films of rizatriptan benzoate, Carbohydr. Polym. 91 (2013) 537–542.
[62] N. Malviya, M.N. Patro, K. Somisetty, K. Vemula, Development of transmucosal patch loaded with anesthetic and analgesic for dental procedures and in vivo evaluation, Int. J. Nanomedicine. 11 (2016) 2901–2920.
[63] A. Shefer, S. Shefer, J. Kost, R. Langer, Structural characterization of starch networks in the solid state by cross-polarization magic-angle-spinning carbon-13 NMR spectroscopy and wide angle X-ray diffraction, Macromolecules 25 (1992) 6756–6760.
[64] Y. Hong, G. Liu, Z. Gu, Recent advances of starch-based excipients used in extended-release tablets: a review, Drug Deliv. 23 (2016) 12–20.
[65] J. Boateng, O. Okeke, Evaluation of clay-functionalized wafers and films for nicotine replacement therapy via buccal mucosa, Pharmaceutics. 11 (2019) 104.
[66] N.S. Mendonsa, P. Thipsay, D.W. Kim, S.T. Martin, M.A. Repka, Bioadhesive drug delivery system for enhancing the permeability of a BCS class III drug via hot-melt extrusion technology, AAPS PharmSciTech. 18 (2017) 2639–2647.
[67] R. Krampe, D. Sieber, M. Pein-Hackelbusch, J. Breitkreutz, A new biorelevant dissolution method for orodispersible films, Eur. J. Pharm. Biopharm. 98 (2016) 20–25.
[68] I. Speer, M. Preis, J. Breitkreutz, Novel dissolution method for oral film preparations with modified release properties, AAPS PharmSciTech. 20 (2019).
[69] P. Costa, J.M. Sousa Lobo, Modeling and comparison of dissolution profiles, Eur. J. Pharm. Sci. 13 (2001) 123–133.
[70] N.A. Nafee, F.A. Ismail, N.A. Boraie, L.M. Mortada, Mucoadhesive buccal patches of miconazole nitrate: in vitro/in vivo performance and effect of ageing, Int. J. Pharm. 264 (2003) 1–14.
[71] Y. Ikeuchi-Takahashi, C. Ishihara, H. Onishi, Evaluation of polyvinyl alcohols as mucoadhesive polymers for mucoadhesive buccal tablets prepared by direct compression, Drug Dev. Ind. Pharm. 43 (2017) 1489–1500.
[72] I.A. Sogias, A.C. Williams, V.V. Khutoryanskiy, Why is chitosan mucoadhesive? Biomacromolecules 9 (2008) 1837–1842.
[73] E. Meng-Lund, J. Jacobsen, A. Müllertz, E.B. Jørgensen, R. Holm, Buccal absorption of diazepam is improved when administered in bioadhesive tablets—An in vivo study in conscious Göttingen mini-pigs, Int. J. Pharm. 515 (2016) 125–131.
[74] M. Jug, M. Bećirević-Laćan, S. Bengez, Novel cyclodextrin-based film formulation intended for buccal delivery of atenolol, Drug Dev. Ind. Pharm. 35 (2009) 796–807.
[75] A. Abruzzo, F. Bigucci, T. Cerchiara, F. Cruciani, B. Vitali, B. Luppi, Mucoadhesive chitosan/gelatin films for buccal delivery of propranolol hydrochloride, Carbohydr. Polym. 87 (2012) 581–588.
[76] M.S. Freag, W.M. Saleh, O.Y. Abdallah, Exploiting polymer blending approach for fabrication of buccal chitosan-based composite sponges with augmented mucoadhesive characteristics, Eur. J. Pharm. Sci. 120 (2018) 10–19.
[77] A. Bernkop-Schnürch, S. Dünnhaupt, Chitosan-based drug delivery systems, Eur. J. Pharm. Biopharm. 81 (2012) 463–469.
[78] A. Miro, A. Rondinone, A. Nappi, F. Ungaro, F. Quaglia, M.I. La Rotonda, Modulation of release rate and barrier transport of Diclofenac incorporated in hydrophilic matrices: Role of cyclodextrins and implications in oral drug delivery, Eur. J. Pharm. Biopharm. 72 (2009) 76–82.
[79] M.S. El-Samaligy, S.A. Yahia, E.B. Basalious, Formulation and evaluation of diclofenac sodium buccoadhesive discs, Int. J. Pharm. 286 (2004) 27–39.